

Biological Mineralization of Hydrophilic Intraocular Lenses

Petros G. Koutsoukos ^{1,*}, Panagiota D. Natsi ¹, Sotirios P. Gartaganis ² and Panos S. Gartaganis ³

¹ Foundation of Research and Technology Hellas-Institute of Chemical Engineering Sciences, FORTH/ICE-HT, University of Patras, 26500 Patras, Greece

² Department of Ophthalmology, School of Medicine, University of Patras, 26500 Patras, Greece

³ Ophthalmology, 251 Hellenic Air Force General Hospital, 11525 Athens, Greece

* Correspondence: pgk@chemeng.upatras.gr; Tel.: +30-6987504842

Abstract: Biomaterials calcify upon implantation in contact with biological fluids, which are supersaturated with respect to more than one crystalline phase of calcium phosphate. The implantation of intraocular lenses (IOLs) for cataract treatment has been hailed as a major advance. Hydrophilic acrylic IOLs, made of Poly(2-hydroxyethyl methacrylate) (PHEMA), upon contact with aqueous humor, exhibit significant incidence of opacification, due to the formation of calcium phosphate crystals, mainly hydroxyapatite ($\text{Ca}_5(\text{PO}_4)_3\text{OH}$, HAP) on the surface or in their interior. The aqueous humor is supersaturated with respect to HAP. Clinical findings were duplicated by laboratory experiments through the development of appropriate experimental models which included batch reactors, well stirred operating at constant supersaturation (CCR) and reactors simulating anterior eye chamber (ECSR). In both CCR and ECSR, simulated aqueous humor was used. In ECSR the flow rate was the same as in the eye chamber (2.5 mL per 24 h). HAP formed both on the surface and inside the IOLs tested. Induction times preceding the crystallization of HAP on the surface of the IOLs and crystal growth rates were measured. Surface hydroxyl ionized groups favored the development of locally high supersaturation by surface complexation. In the interior of the IOLs, HAP formed by the diffusion of the calcium and phosphate ions inside the polymeric matrix.



Citation: Koutsoukos, P.G.; Natsi, P.D.; Gartaganis, S.P.; Gartaganis, P.S. Biological Mineralization of Hydrophilic Intraocular Lenses. *Crystals* **2022**, *12*, 1418. <https://doi.org/10.3390/cryst12101418>

Academic Editors: Ruikang Tang, Blaine Mooers and Jolanta Prywer

Received: 29 August 2022

Accepted: 2 October 2022

Published: 8 October 2022

Publisher's Note: MDPI stays neutral with regard to jurisdictional claims in published maps and institutional affiliations.



Copyright: © 2022 by the authors. Licensee MDPI, Basel, Switzerland. This article is an open access article distributed under the terms and conditions of the Creative Commons Attribution (CC BY) license (<https://creativecommons.org/licenses/by/4.0/>).

Keywords: intraocular lenses; hydrophilic; calcification; kinetics; induction time; zeta potential

1. Introduction

Materials and objects, compatible with human body, needed for the replacement of damaged or malfunctioning parts or tissues in the human body has been the target of intense and innovative research during the past century. Several types of successful biomaterials have thus been developed and manufactured. The compatibility consists in their capability to be accepted by the body when implanted and in contact with other tissues and body fluids. The devices inserted in tissues, made of biomaterials are known as implants. The advent of intraocular lenses (IOLs), revolutionized cataract surgery and they are among the most recently developed implantable biomaterials. Natural lens consists of fiber cells with 65% water content and the rest organic, mainly proteins which give a stable and high refractive index to the lens. The stability of the density of this composite material is responsible for the lens transparency [1]. The earliest IOLs were made of polymethylmethacrylate (PMMA), following the observations of Sir Harold Ridley on fragments of this plastic from the cockpits struck during dogfights, in eyes of the pilots during World War II [2]. Since then, IOL implants have been developed with respect to both functional design and materials used for their construction. PMMA and Poly(2-hydroxyethyl methacrylate) (PHEMA) are the dominant materials used currently following cataract surgery carried out to replace the damaged optical function of the natural lens. The hydrophilicity of PHEMA is due mainly to the hydroxyl groups of the polymer chains and partly to the polar carbonyl groups. The polymer, upon contact and equilibration with water becomes soft and flexible. IOLs made of PHEMA hydrogel are quite popular and the water content ranges between

18–38%. Various biomaterials have been used since 1949, for the fabrication of IOL and since then research is intense concerning materials development and biocompatibility. Over the past two decades, calcification has been reported with a few hydrophilic IOLs, and subsequently, a number of these IOLs were explanted [3–6]. Calcification response after IOL implantation depends on both the composition of the aqueous humor (AH) and on the material of construction of the IOLs. Jenssen et al. [4] reported on the post-operative formation of calcium phosphate deposits on IOLs and attributed it to the viscoelastic material (hyaluronic acid) used during the operation. The mineral deposit however was not characterized by physicochemical methods. Silicon-based IOLs were also reported to be favorable substrates for the development of calcific deposits which were identified by scanning electron microscopy (SEM) and X-ray diffraction (XRD) [5]. It seems that the viscoelastic materials used in ocular surgery in the case of cataract IOL placement which contain sulfate and carboxylate groups facilitate nucleation and subsequent growth of calcium phosphates [6]. The formation of calcium phosphate on implanted biomaterials is the result of the heterogeneous nucleation and subsequent crystal growth of the mineral phase. According to the classical nucleation theory two factors are important: the AH which is supersaturated with respect to calcium phosphate, and the substrate on which the heteronuclei form, which in our case of interest is IOL material [7]. The substrates provide active sites energetically favorable for the initiation of heterogeneous growth of calcium phosphate. From the fact, that hydrophobic IOLs do not calcify practically at all, while hydrophilic IOLs suffer from calcification opacification, which implies vision complications and replacement difficulties, it may be suggested that the structure of the IOL material plays an important role in the formation and further development of mineral deposits on, inside, or in both places of IOLs [8,9]. In this work we present an investigation on the mechanism of the formation of calcium phosphate deposits on the IOLs, based on kinetics data of the calcification process, obtained from experimental models, which simulate the conditions in human eye. In the models we have used, hydrophilic IOLs were in contact with simulated aqueous humor which is supersaturated with respect to hydroxyapatite ($\text{Ca}_5(\text{PO}_4)_3\text{OH}$, HAP). Two experimental models were used: (a) glass reactors in which the formation of calcium phosphate on hydrophilic IOLs was investigated at constant supersaturation (Constant Composition Reactors, CCR) monitoring the rate of proton release in the solution due to the precipitation of HAP [10], and (b) reactors simulating eye chamber (Eye Chambers Simulation Reactor, ECSR) in which the composition of the aqueous phase, simulated the corresponding to AH and the respective flow was the mean physiological, i.e., 2.5 mL per 24 h CCR allow for precise and highly reproducible measurements of the induction times preceding the formation of calcium phosphate and accurate and reproducible measurements of the rates, from which mechanistic information may be obtained through their correlation with the solution supersaturation with respect to the crystal phase forming. Since it is established that the presence of ionizable functional groups on polymers is very important for the initiation of the formation of nuclei of sparingly soluble salts and their subsequent crystal growth, the role of surface charge of PHEMA IOLs was also investigated from measurements of the electrokinetic (zeta) potential [11]. ECSR calcification data at very low flow conditions (mean of the flow rate in normal human eyes) are expected to shed light on the clinical findings which show the formation of HAP in the interior of the IOLs [12]. The aim of the present work was to investigate the mechanism of hydrophilic IOL opacification due to the formation of calcium phosphate deposits on their surface and/or the interior. Measurements of the rates of crystalline material formation and their correlation to the solution supersaturation provide information on the predominant crystal growth mechanism. Moreover, we aimed at replicating clinical findings of the formation of calcific deposits inside the hydrophilic IOLs using composition and flow conditions of the AH similar to the corresponding in the physiological eye and at proposing a feasible mechanism of formation of the calcific deposits.

2. Materials and Methods

All solutions were prepared using triply distilled, deionized water (TDDW). Stock solutions of calcium and phosphate were prepared from crystalline calcium chloride ($\text{CaCl}_2 \cdot 2\text{H}_2\text{O}$) and sodium dihydrogen phosphate (NaH_2PO_4) (Puriss. Merck KGaA, Darmstadt, Germany). Calcium chloride solutions were standardized with standard EDTA solutions (Merck) using murexide indicator and by atomic absorption spectrometry (air-acetylene flame, Perkin Elmer AAnalyst 300, Norwalk, CT, USA). The phosphate stock solutions were standardized with potentiometric titrations with standard sodium hydroxide solutions (Titrisol, Merck KGaA, Darmstadt, Germany) and by spectrophotometric analysis using the vanadomolybdate method spectrophotometrically (Perkin Elmer lambda 35, Norwalk, CT, USA) [13]. Sodium chloride stock solutions were prepared from the crystalline solid, without any further purification. The standard sodium hydroxide solutions used for pH adjustment were checked regularly with potentiometric titrations of carefully weighted quantities of potassium hydrogen phthalate dried previously overnight at 105°C .

2.1. Mineralization Experiments

2.1.1. Constant Composition Reactor (CCR)

The supersaturated solutions were prepared in a water jacketed, double walled borosilicate glass reactor, thermostated by circulating water from a thermostat and the temperature of the solutions in the reactor was constant at $37.0 \pm 0.1^\circ\text{C}$. Equal volumes, 0.100 dm^3 each, of calcium chloride and sodium dihydrogen phosphate were mixed simultaneously in the reactor under stirring with a magnetic stirrer and a Teflon coated stirring bar. The solution pH was adjusted to 7.40 by the addition of standard sodium hydroxide solution. The pH measurements were carried out by a combination glass//Ag/AgCl electrode (GCE) standardized before and after each experiment with standard NIST buffer solutions (pH 4.006, pH 6.865, pH 9.180) [14]. The ionic strength of the supersaturated solutions was adjusted to 0.15 M with NaCl from the respective stock solutions. The final concentrations of total calcium, Ca_t , and total phosphate, P_t , were at levels ensuring that the driving force for the formation of calcium phosphates was the same as in healthy humans [15,16]. Before, during and after pH adjustment of the supersaturated solutions, inert atmosphere over the solution was ensured by pumping through the solutions, pure nitrogen (99.99%, Linde Hellas, Ltd., Schematari, Greece) saturated with water vapor. Following the verification of the stability of the supersaturated solutions, as shown by the stability of the adjusted pH value for at least two hours, a set of hydrophilic IOL lenses (3–5), mounted firmly on a special holder which allowed exposure of both the anterior and the posterior sides, were immersed in the supersaturated solution. The pH of the solutions was monitored. The electrode was connected with the controller unit, which in turn communicated with a computer with the appropriate data acquisition card and with a motorized stage which could move two mechanically coupled, calibrated precision borosilicate glass syringes. The onset of precipitation was marked by drop of the solution pH due to proton release, accompanying the formation of the solid precipitate, as, e.g., in the case of hydroxyapatite ($\text{Ca}_5(\text{PO}_4)_3\text{OH}$, HAP) shown in Equation (1) [17,18]:



Drop of the solution pH by about the sensitivity limit of measurement of the GCE, i.e., ca. 0.005 pH units, triggered the addition of equal volumes from the two syringes. The two syringes contained solutions, the composition of which was calculated on the basis of the stoichiometry of the precipitating solid, i.e., $\text{Ca}:\text{P}:\text{OH} = 5:3:1$. Specifically, the composition of the titrant solutions was:

Syringe 1: calcium chloride solution and sodium chloride, $(2 \times \text{Ca}_s + m) + (2 \times \text{C}_{\text{NaCl},s} - 2m)$ where subscript s denotes the corresponding concentration in the supersaturated solutions and m is an arbitrary constant determined by preliminary experiments) Syringe

2: sodium dihydrogen phosphate, sodium hydroxide, $(2 \times C_{\text{NaH}_2\text{PO}_4,s} + n) + (2 \times C_{\text{NaOH},s} + 2m - n)$, where n is a constant such that $\frac{m}{n} = \frac{5}{3}$.

The composition of the titrant solutions 1 and 2 was selected appropriately to maintain the activities of the ion species in the supersaturated solutions throughout the precipitation of HAP. In our experiments, according to series of preliminary experiments, best results were obtained for $m = 10 \times C_{a_s}$. Since titrant solutions replace the aqueous species transferred to the solid phase, it is obvious that the rate of their addition (mL/s) is directly related with the number of HAP of moles precipitated per s. Monitoring therefore the volume of titrants added, from the beginning of immersion of the IOLs in the supersaturated solutions (time, $t = 0$), it is possible to measure accurately the induction time (time lapsed from $t = 0$, till time t , when addition of titrants started) and the rates of the solid precipitation, from the slope of the respective volume- time profiles (moles HAP/s). The application of the constant supersaturation method is important for the improvement of the accuracy of the measurement of induction times, because the measurements are carried out at the same driving force. Relying simply on pH change monitoring, the onset of changes of pH coincides with the solution de-supersaturation and the respective measurements do not correspond to the same driving force, which affects strongly this induction time, especially at low supersaturations. The experimental set up, used for the investigation of the kinetics of mineralization of hydrophilic IOLs is shown in Figure 1.

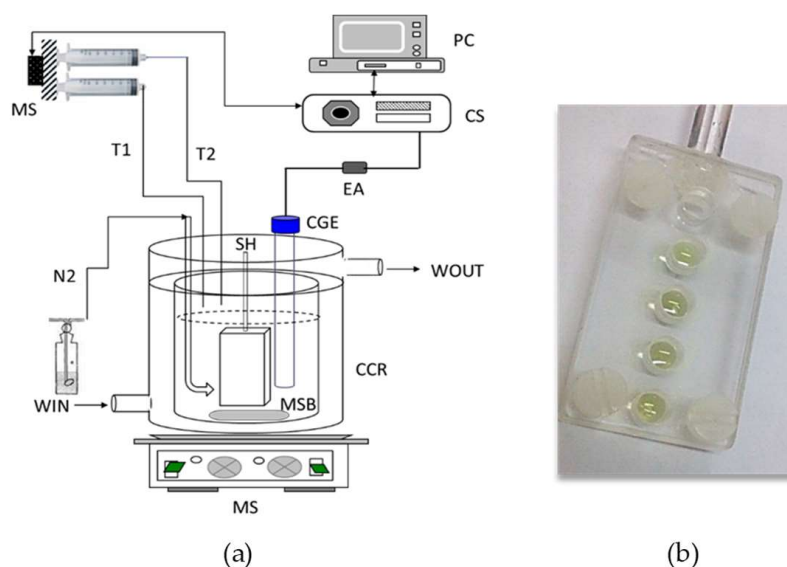


Figure 1. Experimental setup for the study of kinetics of calcification of IOLs. (a): CCR: constant composition reactor (dotted circle shows the level of the supersaturated solution simulating aqueous humor); MS: magnetic stirrer; MSB: Teflon coated magnetic stirring bar; WIN, WOUT, inlet and outlet, respectively, of water from the thermostat; N2: water vapor saturated nitrogen to maintain inert atmosphere in the reactor; SH: holder for the IOLs; GCE: glass- Ag/AgCl combination electrode; EA: GCE electrode amplifier; CU: control unit interfaced with computer (PC) and the motorized double syringe system (MS); T1, T2: lines for the addition of titrant solutions 1 and 2 in the CCR; (b): Photo of the IOLs mounting system with mounted IOLs.

Typical titrant addition plots, from which the induction time (t_{ind}) and the rate of HAP formation on the IOLs were calculated, is shown in Figure 2:

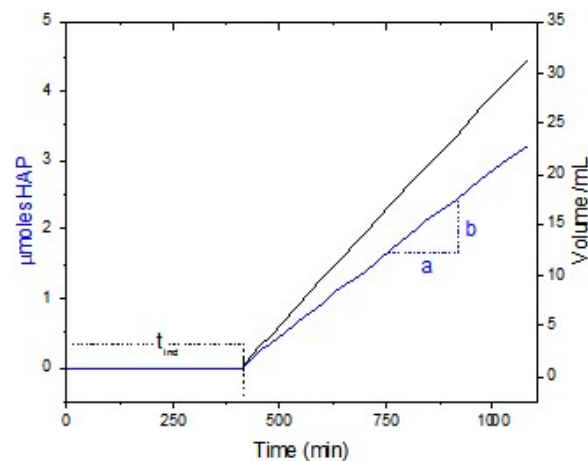


Figure 2. Recording of the volume (—) of titrant solutions added to keep supersaturation constant and calculated mass of HAP (—) deposited on hydrophilic IOLs.

The rates of HAP precipitation were precipitated from the slope b/a normalized for the total surface area, SA , of the exposed IOLs:

$$\text{Rate of precipitation} = \frac{b}{a} \times \frac{1}{SA} \quad (2)$$

Whereas SA was taken the geometric surface area of the IOLs exposed to the supersaturated solutions. It should be noted that the SA of each IOL (both sides) was taken as ca. 2 cm^2 .

2.1.2. Eye Chamber Simulating Reactor (ECSR)

This type of reactor was constructed to provide a better simulation of the eye chamber. In this reactor, it was possible to monitor the process of calcification of IOLs both sides of which were exposed to simulated aqueous humor (SAH, Table 1), which is supersaturated with respect to HAP. The ECSR, was constructed of polyamide and it was double-walled, so that water from a thermostat circulated with the help of a pump keeping the temperature of the solutions inside the reactor at $37.0 \pm 0.5 \text{ }^\circ\text{C}$. The temperature control of the SAH inside ECSR was tested through measurements of SAH flowing through the ECSRs with thermocouples and digital thermometers in the sequence of 3 ECSRs used. Moreover, during the entire duration of the experiments, the temperature of the exiting from the last ECSR SAH was monitored with a thermocouple thermometer. The total volume of the reactor was ca. 10 mL. Glass windows on the top and the bottom of the reactors allowed direct visualization inside the reactor using a microscope with a camera capable of picture recording. A set of three reactors in series was used to check reproducibility. Sampling both at the inlet and the outlet of the reactors showed that the concentrations of the ions responsible for the formation of the calcific deposits (calcium and phosphate) and the pH remained constant in the fluid phase. This meant that in the event of calcification of the IOLs exposed inside the ECSRs, the flow rate was sufficient to make up for the concomitant transfer of these ions to the solid phase. The SAH circulated through the reactors, contacting both sides of the exposed IOLs, at a rate of 0.2 mL/h. This flowrate is the average value for human eye at physiological conditions. Three IOLs were introduced in each reactor using a special holder, allowing the exposure of both sides of the IOLs to SAH. Simulated aqueous humor (SAH) was prepared from stock solutions of sodium bicarbonate, magnesium chloride, calcium chloride, potassium chloride, disodium hydrogen phosphate and sodium chloride, so that the final concentration was as shown in Table 1 [14].

Table 1. Components and respective concentrations of the simulated aqueous humor (SAH)¹.

Component	Formula	Concentration/mM
Disodium hydrogen phosphate	Na ₂ HPO ₄	0.6
Magnesium Chloride	MgCl ₂	1.0
Sodium bicarbonate	NaHCO ₃	33.6
Calcium Chloride	CaCl ₂	1.7
Potassium Chloride	KCl	5.3
Sodium Chloride	NaCl	150.0

¹ Composition refers to inorganic components only and is the same as in normal humans' aqueous humor.

For each series of experiments the hydrophilic IOLs placed in the holders were identical (shape, water content, and production batch) and they all were products for direct consumption taken from their packages. The ECSR and the IOL holder is shown in Figure 3.

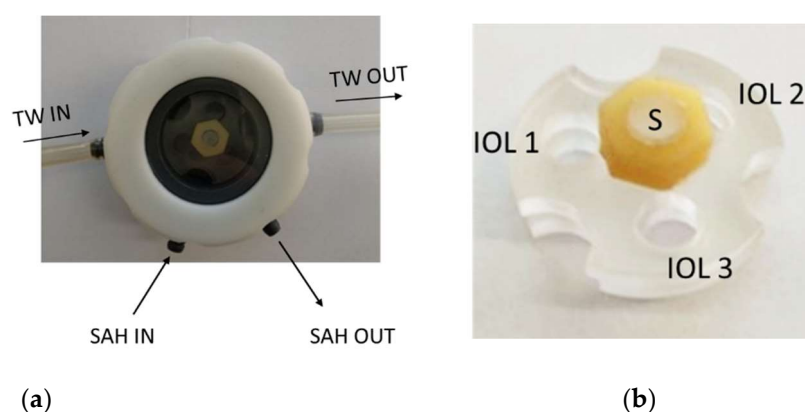


Figure 3. (a). Eye chamber reactor; TW IN, TW OUT: inlet and outlet of water from thermostat at 37 °C. (b). Holder for IOLs inside ECSR; S: securing bold and nut to keep in place IOLs.

The progress of the formation of deposits was first observed by optical microscopy (Olympus CH2 microscope model CHT with video camera, Olympus Optical Co., Ltd. (EUROPA GMBH, Hamburg, Germany) and quantified by optical density measurements (Perkin Elmer lambda 35, Norwalk, CT, USA) at 650 nm. The total duration of the calcification measurements in the ECSRs lasted up to 12 months. Removal of IOL samples to examine the progress of calcification was carried out either every 10 days (duration of 3 months total) or every 40 days (duration 12 months). During this period and every 4 days, fresh SAH solutions were prepared and pumped in the ECSRs containing the hydrophilic IOLs.

2.2. Solids Characterization

The solids formed on the surface of the IOLs were characterized by scanning electron microscopy (SEM, LEO SUPRA 35VP, Zeiss Oberkochen, Germany with a microanalysis probe, BRUKER AXS, Billerica, MA, USA). Microraman spectrometry was also used for the identification of the mineral deposits. For control purposes stoichiometric HAP solids were used. The mineral phase was identified in this case by powder X-ray diffraction (D-5000, Siemens Frankfurt, Germany). The zeta potential of the IOLs was calculated from measurements of the streaming potential in a homemade apparatus [19]. The hydrophilic IOLs were cut in ca. 1 mm pieces and were packed in the measurement cell (porous plug). Electrolyte flow through the plug was achieved by the application of pressure difference, ΔP , at the ends of the cell by nitrogen gas. The resulting streaming potential, E_s , was recorded by a digital high impedance voltmeter connected with a computer. The specific conductivity of the solutions was measured with a conductivity meter (CDM 712,

Metrohm AG, Zurich, Switzerland). For each electrolyte concentration measurements were conducted at six different pressures. The ζ potential was calculated by the Smoluchowski equation [19].

3. Results

3.1. IOL Calcification in the CCR-Measurement of Kinetics

All IOLs investigated were hydrophilic (PHEMA) with water content of 26%. In all cases rather long induction times were measured before the onset of the formation and development of calcium phosphate which was identified as HAP. It is interesting to note that the method of fixing water content did affect the induction times measured and the rates of the subsequent crystal growth of HAP. The dependence of the induction time in turn on the solution supersaturation, implied differences in the surface energy of the IOLs. IOLs hydrated by immersion and treatment with water, borate buffer solution (BBS, 39.9 mM boric acid, 0.37 mM sodium tetraborate and 137 mM sodium chloride, pH 7.40) and Phosphate buffer solution (PBS, sodium phosphate dibasic 3.38 mM, disodium phosphate monobasic, 142 mM sodium chloride, pH 7.40) were tested and the results are summarized in Table 2.

Table 2. Calcification of hydrophilic IOLs at constant supersaturation; Total calcium, $Ca_t = 1.70$ mM, total phosphate, $P_t = 1.02$ mM, NaCl 150 mM, pH 7.40, 37 °C; hydration/storage medium, induction times and rates of HAP formation.

Hydration/Storage Solution	Induction Time, t_{ind} (min)	Surface Energy, γ_s ($\text{mJ}\cdot\text{m}^{-2}$)	Precipitation Rate *, R_p / $\times 10^{-4}$ $\text{molHAP}\cdot\text{min}^{-1}\cdot\text{m}^{-2}$
Water	37	39	4.70
PBS	225	42	0.90
BBS	360	50	0.01

* Rates reported per unit geometric surface area of the IOLs.

The calculations of the surface energy were based on the dependence of the induction time preceding the precipitation of HAP on the solution supersaturation, as detailed in the discussion section (Equation (7)).

The effect of the storage medium on the induction time and the subsequent HAP formation rates on the IOLs is shown in Figure 4.

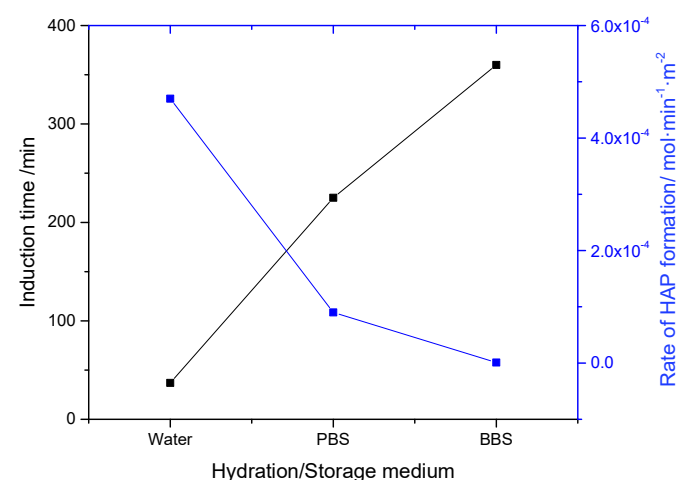


Figure 4. The effect of hydration/storage medium on the induction times and the rates of HAP formation on hydrophilic IOLs; Total calcium, $Ca_t = 1.70$ mM, total phosphate, $P_t = 1.02$ mM, NaCl 150 mM, pH 7.40, 37 °C.

The morphology of the precipitates formed on the IOLs treated with the different hydration media is shown in Figure 5.

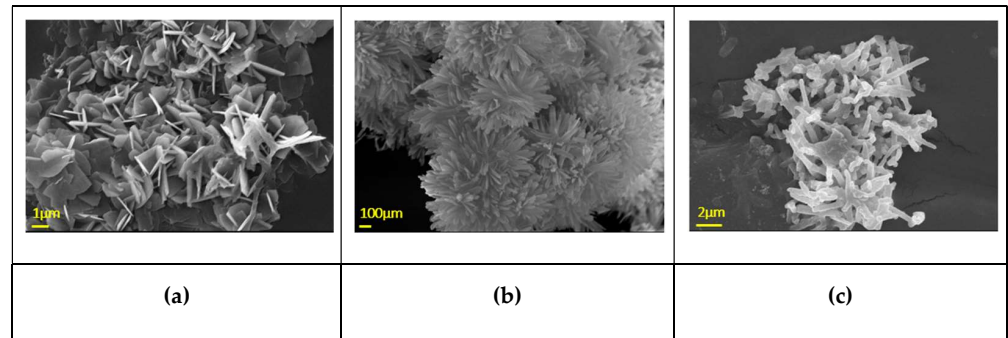


Figure 5. SEM photos of apatitic deposits on calcified IOL surface IOLs hydrated with different solutions; (a) Water; (b) Phosphate Buffer Solution (c) Borate Buffer Solution; pH 7.4, 37 °C, 0.15 M NaCl.

In all cases crystalline deposits of HAP were obtained. It should be noted that tripling the total surface area of the IOLs in contact with the mineralization solution, the rates were tripled, while the induction time remained the same. It was thus confirmed that calcification took place exclusively on the IOLs and not on the bulk solution (secondary growth). The driving force for the nucleation and crystal growth of HAP on the IOLs is the Gibbs free energy change for going from the supersaturated solution to equilibrium with respect to the precipitating phase, HAP in this case, ΔG_{HAP} :

$$\Delta G = -\frac{R_g T}{9} \ln \frac{\alpha_{Ca^{2+}}^5 \alpha_{PO_4^{3-}}^3 \alpha_{OH^-}}{K_{s,HAP}^0} \quad (3)$$

where R_g is the gas constant, T the absolute temperature, α , the ion activity of the subscripted ion and $K_{s,HAP}^0$ the thermodynamic solubility product of HAP. The logarithmic term is defined as the supersaturation ratio with respect to HAP, S_{HAP} .

$$S_{HAP} = \frac{\left(\alpha_{Ca^{2+}}^5 \alpha_{PO_4^{3-}}^3 \alpha_{OH^-} \right)}{K_{s,HAP}^0} \quad (4)$$

The relative supersaturation with respect to HAP, σ_{HAP} is:

$$\sigma_{HAP} = S_{HAP}^{\frac{1}{9}} - 1 \quad (5)$$

The rates of HAP formation varied also as a function of the solution supersaturation. The dependence of the measured rates of HAP precipitation on HAP crystals (reference material) and on PHEMA IOLs, as a function of the relative supersaturation are shown in Figure 6.

Dense crystalline HAP crystal layers were formed on the surface of the IOLs, which showed a leaflet morphology, like the reported for the crystal growth of HAP in simulated body fluid (SBF) [20]. The morphology of the grown crystals is shown in Figure 7.

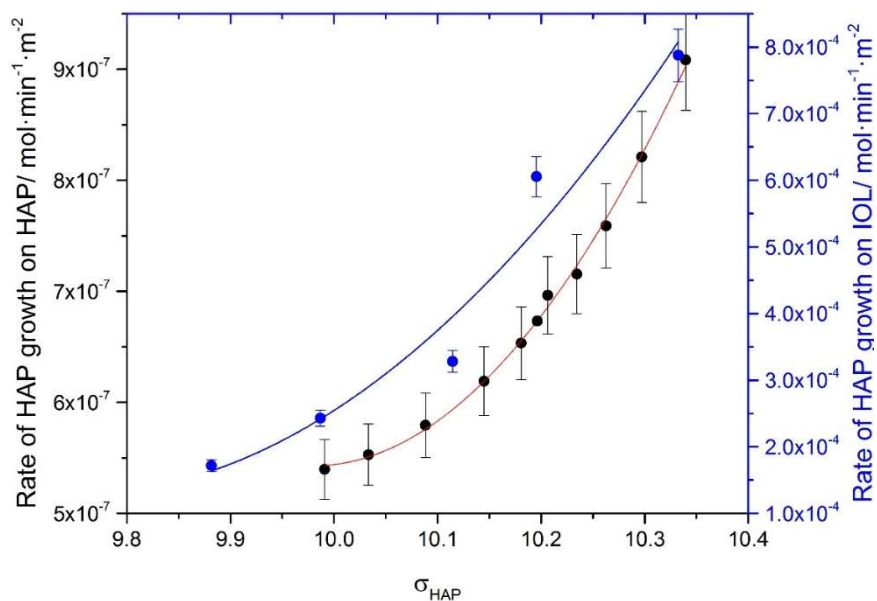


Figure 6. Rate of HAP crystal growth from supersaturated solutions as a function of the relative solution supersaturation with respect to hap; pH 7.40, 150 mM NaCl; (●) HAP seeds. Rates expressed per unit surface area measured by BET nitrogen adsorption method (●) rates expressed per unit geometric surface area of the hydrophilic IOLs in contact with the supersaturated solutions.

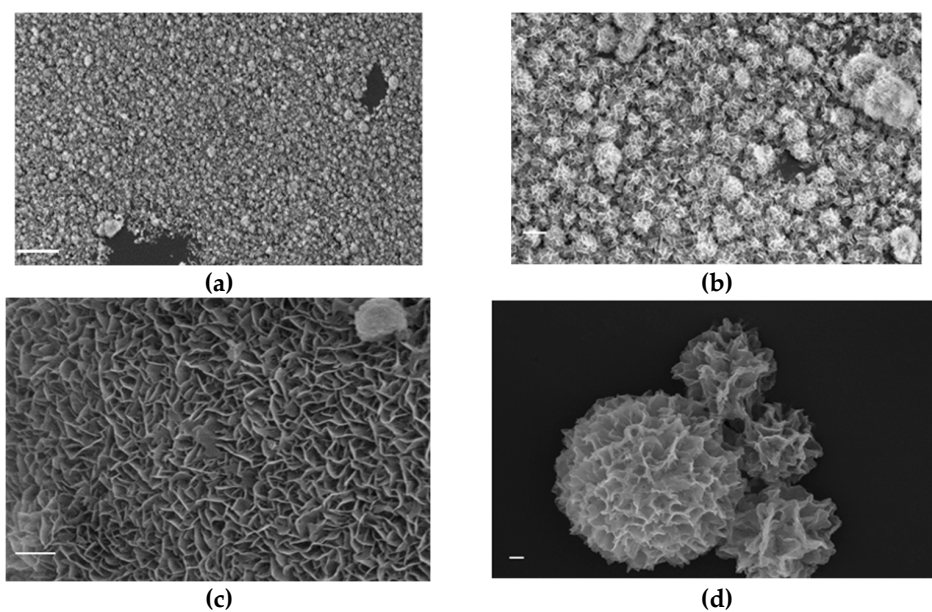


Figure 7. HAP crystals formed on hydrophilic IOLs at constant supersaturation; pH 7.40, 37 °C, 0.15 M NaCl. (a) bar 10 μm; (b) bar 2 μm; (c) bar 1 μm; (d) bar 200 nm.

EDX microanalysis, confirmed the formation of calcium phosphate as may be seen in Figure 8.

Micro-Raman analysis of the deposits confirmed the presence of the characteristic bands corresponding to PO_4 groups stretching, as may be seen in Figure 9.

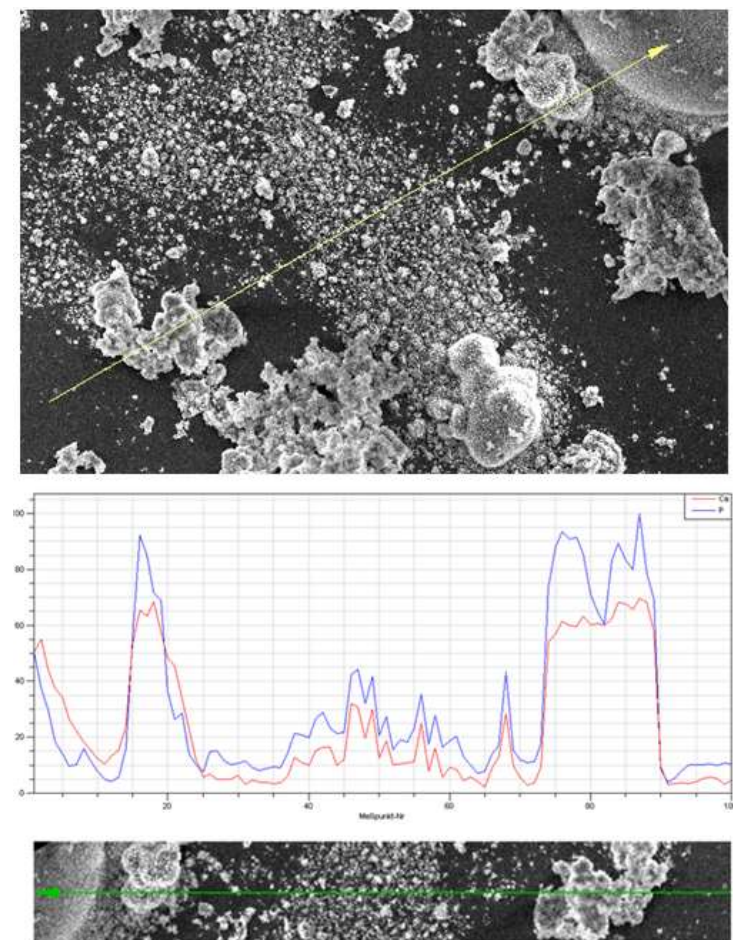


Figure 8. Line scan microanalysis of deposits formed on hydrophilic IOLs at constant supersaturation; upper figure SEM of the deposits with the yellow line showing the location of line scan analysis; lower figure shows the result of line scan analysis (red line for element Ca and blue line for element P); below line scan analysis the magnified SEM picture shows the exact path of microanalysis line scan; pH 7.40, 37 °C, 0.15 M NaCl.

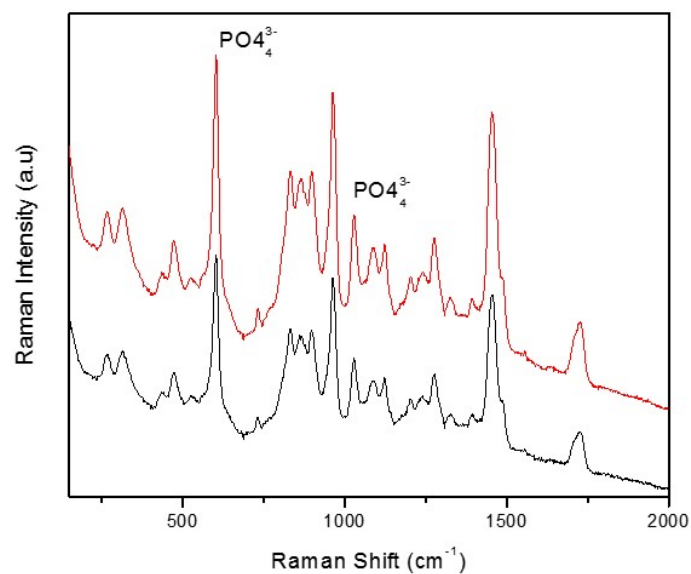


Figure 9. Micro-Raman spectra from two spots of mineral deposits formed on hydrophilic IOLs at constant supersaturation. pH 7.40, 37 °C, 0.15 M NaCl.

The bands at 960 cm^{-1} are characteristic for HAP. It should be noted however that, this band is in between the bands corresponding to octacalcium phosphate ($\text{Ca}_4(\text{PO}_4)_3\text{H}\cdot 2.5\text{H}_2\text{O}$, OCP), a metastable crystal phase of calcium phosphate [21,22]. Despite this fact in combination with equilibrium calculations which showed that the conditions in the solutions used to simulate aqueous humor, corresponded to supersaturation only with respect to HAP (Figure S1, Supplementary Material) thus precluding the formation of OCP. X-ray diffractograms were noisy because of the small quantities involved and the polymer matrix but they showed the characteristic reflections (002) and (211) of HAP (Figure S2).

The most interesting feature however was that besides the formation of HAP on the surface of the IOLs tested, examination of cross sections of mineralized IOLs revealed the formation of the same mineral at various depths. As may be seen in Figure 10, denser HAP formations were observed ca. $20\ \mu\text{m}$ from the anterior surface of the IOL, with the formations becoming sparser at higher depths.

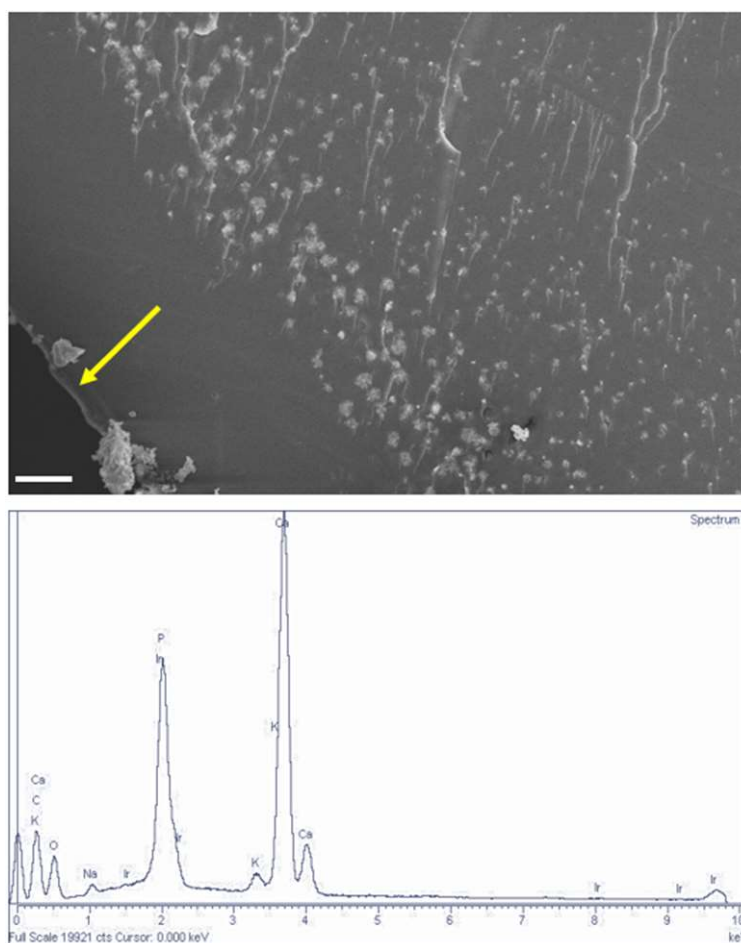


Figure 10. HAP formation in the interior of IOL mineralized in the CCR; pH 7.40, $37\ ^\circ\text{C}$, 0.15 M NaCl. Arrow shows the anterior surface of the IOL. Bar $10\ \mu\text{m}$. EDS spectrum below the SEM picture shows the result of the microanalysis which included the entire area of the SEM picture above.

3.2. IOL Calcification in the ECSR

As already mentioned, the progress of mineralization in the ECSR was carried out by exposure of the hydrophilic IOLs in SAH for long periods of time. Samples were removed periodically to assess the progress of the deposits. At a first stage, the progress of calcification was monitored by in situ examination of the test specimens under the optical microscope (OM). In Figure 11, a typical picture is shown from OM pictures over a period of 12 months.

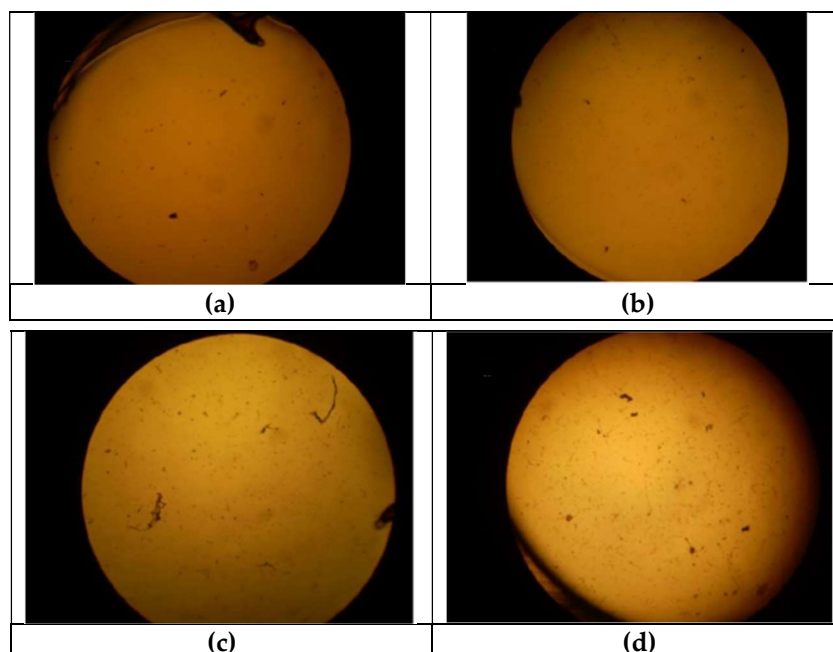


Figure 11. Optical images from IOLs in the ECSR, exposed in SAH at a flow rate of 2.0 mL/24 h, $\times 40$; pH 7.40, 0.14 M NaCl, 37 °C. (a) residence time 1 month; (b) residence time 5 months; (c) residence time 9 months; (d) residence time 12 months.

It was attempted to quantify the extent of the formation of deposits, measuring the optical density of the IOLs at 650 nm. A linear relationship was found for a period up to 30 days, as may be seen in Figure 12. Past this time the sensitivity of the measured optical density as a function of the surface coverage showed saturation. Optical density measurements of the IOLs may be used for the initial, important stages of calcification to estimate rates, but still more work is needed in this direction.

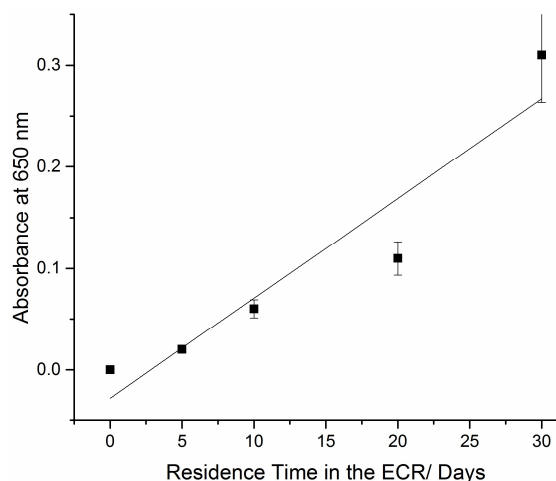


Figure 12. Absorbance of light at 650 nm by IOLs in the ECSR, exposed in SAH at a flow rate of 2.0 mL/24 h, as a function of time; pH 7.40, 0.14 M NaCl, 37 °C.

The surface texture of the IOLs changes drastically as a result of the calcification process as may be seen in the pictures shown in Figure 13. The optical appearance of the IOLs tested before (a) and after (b) calcification over a period of 12 months corresponded to the absence of any deposit (c) and to the presence of deposits which appeared as lumps (d). The lumps consisted of calcium phosphate which was formed both inside the IOLs but also on their surface.

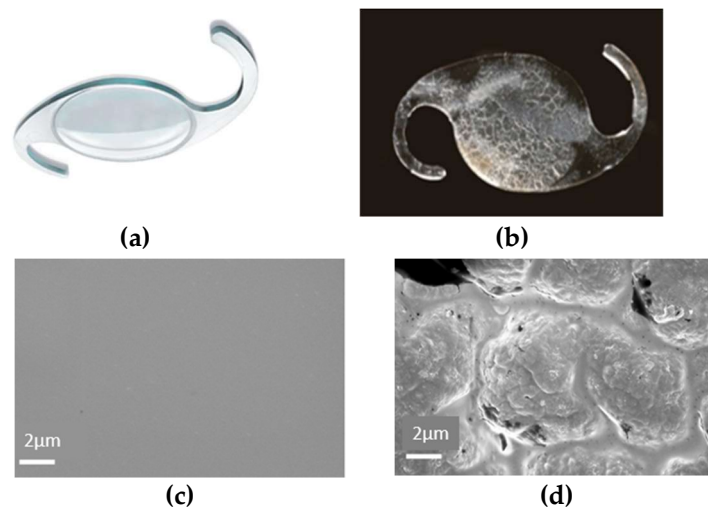


Figure 13. Visual observation of hydrophilic IOL before (a) and after calcification (b) in the ECSR and the respective SEM pictures (c,d).

Similar morphology was obtained from the examination of clinical findings, from IOLs explanted surgically in order to be replaced because of complete opacification which occurred 6 year past their implantation, as may be seen in Figure 14.

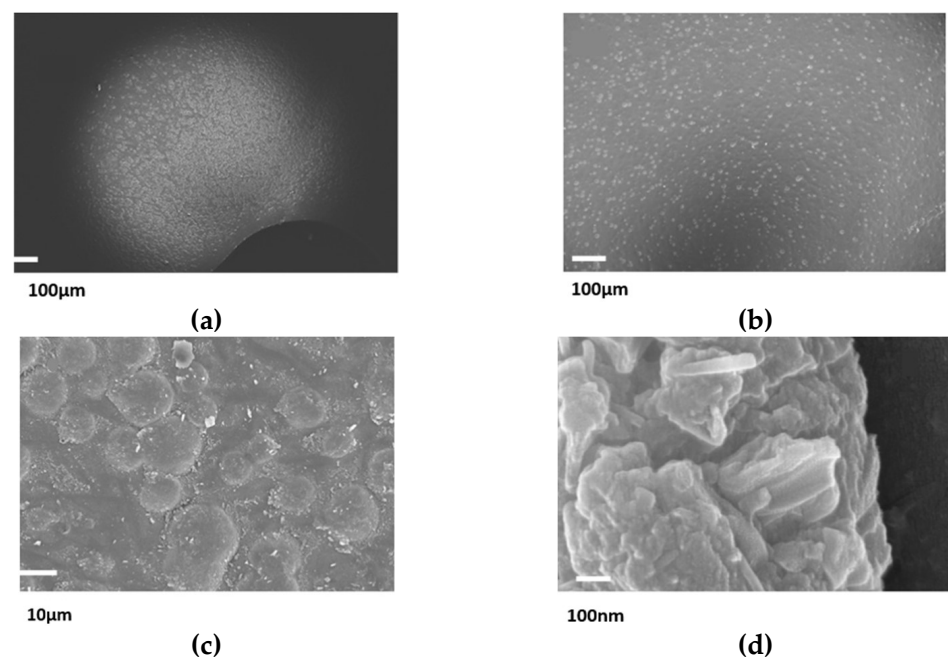


Figure 14. SEM pictures of hydrophilic IOL extracted after opacification, six years past implantation. Deposits of calcium phosphate formed in the haptics (a,b) and in the anterior of the IOL (c,d). The lumps seen are formed because of HAP deposits under the surface of the IOL.

4. Discussion

The results presented above showed that the two types of reactors, can simulate satisfactorily the *in vivo* IOL opacification. Each type of reactor has its specific advantages. The kinetics of IOL calcification was measured with high accuracy and reproducibility and were correlated with the driving force for the mineral growth to understand the dominant mechanism for the formation of HAP. Measurements of the induction time and of the rates of mineralization in the CCR and the use of equations from the classical nucleation theory (CNT) [23,24], yielded estimates of the surface energy of the growing nuclei. the calculated values of surface energy provided some insight, related with the energy barrier for the

formation of stable nuclei on the surface of the IOL which calcify in solutions, simulating AH. According to the CNT there is an energy barrier for the formation of a critical nucleus in the supersaturated solutions. Once formed, the critical nucleus grows further forming crystals which reach macroscopic size. The critical energy, ΔG_{r^*} , corresponding to the formation of a critical nucleus, of radius r^* , is:

$$\Delta G_{r^*} = \frac{16\pi v_m^2 \gamma_s^3}{3(kT \ln S)^2} \quad (6)$$

where v_m and γ_s are the molecular volume and the surface energy of the solid phase forming from the supersaturated solution, k is the Boltzmann constant, T the absolute temperature and S the solution supersaturation with respect to the forming solid. Since the rate of nucleation is exponentially proportional to ΔG_{r^*} and the induction time is inversely proportional to the nucleation rate, the induction time is related to the supersaturation needed for the formation of a nucleus of the solid phase with critical size is given by Equation (7):

$$\log t_{ind} = A + \frac{\beta v_m^2 \gamma_s^3}{(2.303kT)^3} \cdot \frac{1}{\log^2 S} \quad (7)$$

where A is a constant, and β , a shape factor ($16\pi/3$ for spheres). The values of the surface energy of HAP forming on the hydrophilic IOLs, reported in Table 2 were calculated according to Equation (7). The surface energy of a nucleus growing on a substrate depends on the aqueous medium and on the substrate, as may be seen in Figure 15.

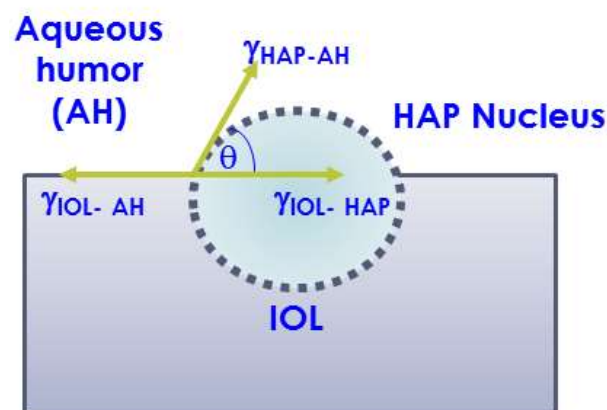


Figure 15. Model for the heterogeneous nucleation of HAP on IOLs. The vectors of the interfacial energies IOL-HAP, IOL-AH, HAP-AH and the contact angle are shown.

The presence of PHEMA in the aqueous humor, which is supersaturated with respect to HAP, plays a catalytic role, facilitating the formation of a spherical cap nucleus, instead of a nucleus represented by the entire sphere. It is for this reason that the energy barrier for homogeneous nucleation (Equation (6)) is higher than the corresponding for heterogeneous nucleation, $\Delta G_{r^*,het}$. The free energy change needed for homogeneous (ΔG_{r^*}) and heterogeneous nucleation free energy change, ($\Delta G_{r^*,het}$) are related with Equation (8):

$$\Delta G_{r^*} = \varphi \Delta G_{r^*,het} \quad (8)$$

where φ is a factor related with the contact angle θ :

$$\varphi = \frac{(2 + \cos \theta)(1 - \cos \theta)^2}{4} \quad (9)$$

The parameter φ , according to Equation (9), takes values 0–1. $\varphi = 1$ when $\theta = 180^\circ$. This corresponds to a completely non-wetting situation, which corresponds to lack of affinity between the substrate and the overgrowth. On the other hand, $\varphi = 0$ when $\theta = 0$, i.e., when

there is full compatibility between the substrate and the overgrowth. This case corresponds to seeded crystal growth (as in Figure 6 for HAP seed crystals) in which there is no energy barrier for nucleation. According to the model shown in Figure 15, $\cos\theta$, can be calculated from the synthesis of the interfacial energy vectors involved:

$$\gamma_{IOL-AH} = \gamma_{HAP-IOL} + \gamma_{HAP-AH} \cos\theta \Rightarrow \cos\theta = \frac{\gamma_{IOL-AH} - \gamma_{HAP-IOL}}{\gamma_{HAP-AH}} \quad (10)$$

According to the results shown in Table 2 and Figure 4, higher surface energy values resulted to lower rates of HAP formation. The lower rates of formation of HAP on the IOL polymer resulted in the formation of well-shaped prismatic nano crystals of HAP. Higher rates resulted in the formation of HAP nano-plates (Figure 5). The different methods of hydration especially when involving phosphate or borate which may bind on the surface of PHEMA at the hydroxyl or carbonyl group sites are expected to affect the surface energy of the substrates, as it is reflected in the measured induction composition times. The fact that the rates of precipitation, for the same driving force were so different is impressive and it may be suggested that the nucleation process is very important in the overall HAP formation process. Different surface composition (e.g., in the presence of adsorbates) is expected to affect the nucleation barrier. According to the CNT, the rate of nucleation is inversely proportional to the surface energy of the solid substrate [25].

The parabolic dependence of the rates of HAP precipitation (Figure 6), on the relative supersaturation suggested HAP growth both on the HAP seeds and on the IOLs, suggested that the mechanism was the same, i.e., the formation of HAP in the IOLs was surface diffusion controlled. The difference in the growth rate constants cannot be assessed because of the different surface area reference. In the case the rates of crystal growth of HAP on HAP were normalized per unit surface area, which was calculated based on the specific surface area (m^2/g) measured by nitrogen absorption (BET method). For the growth of HAP on the IOLs, their total geometric surface area was considered for the normalization of the rates per unit surface area. The mechanism of HAP formation the IOLs, implied that their polymeric surface plays an important role. The surface of PHEMA (Figure 16) at the physiological pH (7.4) is rich in hydroxyl groups which are ionized [26].

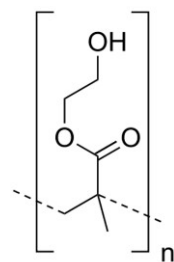


Figure 16. PHEMA molecule, consisting of n HEMA monomers.

As may be seen, the PHEMA monomers, possess -OH groups which may be protonated or deprotonated depending on the solution pH. Additional negatively charged sites are the -C=O groups where excess of electron charge is present at the electronegative oxygen atom. The zeta potential measurements confirmed that, PHEMA at neutral pH has a highly negative charge, as may be seen in Figure 17.

As may be seen from Figure 17, at the physiological pH the surface potential of the IOLs is ca. 100 mV, rather highly negative. At these conditions it is expected that the surface of the IOLs is screened by the Ca^{2+} counter ions, which may form surface complexes with the $-\text{O}^-$ groups of the polymer, creating thus active sites for nucleation and crystal growth of HAP. A schematic illustration of the suggested mechanism for the calcification of IOLs is shown in Figure 18.

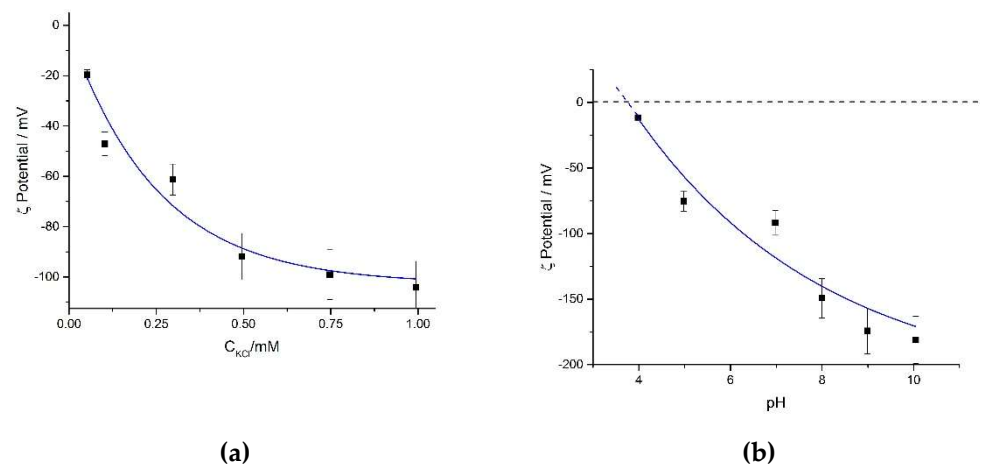


Figure 17. ζ -potential of PHEMA hydrophilic IOLs. (a) pH 7.0, 25 °C; variation of ζ potential as a function of electrolyte concentration; (b) variation of ζ potential as a function of pH; 25 °C, 0.5 mM KCl.

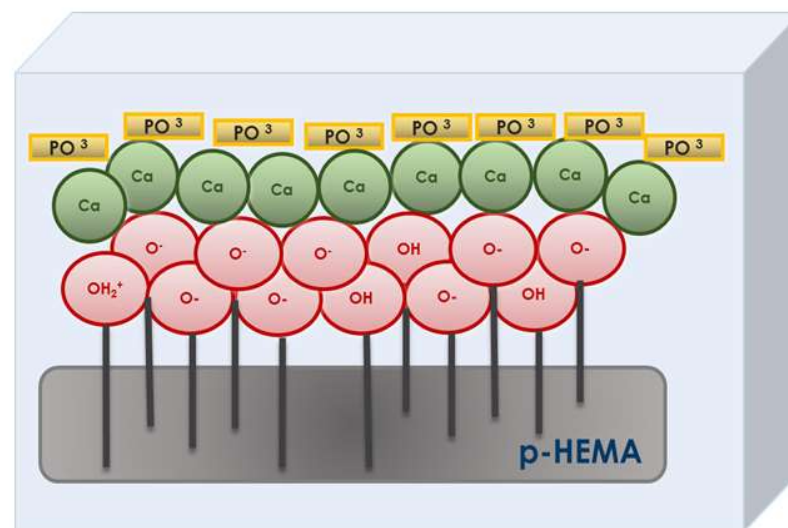


Figure 18. Model for the development of active sites for the nucleation and growth of HAP on hydrophilic IOLs made of PHEMA.

It may be suggested that the accumulation of the oppositely charged Ca²⁺ ions to the PHEMA surface, in combination with the presence of phosphate ions may result to locally high supersaturation, developed in the compact electrical double layer (Stern) domain, which triggers the nucleation and crystal growth of HAP.

The interesting feature of the appearance of HAP crystals in the interior of the IOLs, shown in Figure 10, may be explained by a similar reasoning. The difference, however, is that the supersaturation in the interior is developed by the diffusion of the HAP lattice ions. The fact that these ions are expected to penetrate the polymer matrix from both the posterior and the anterior sides of the IOLs may explain the appearance of fronts of denser crystallite layers (corresponding apparently to higher supersaturation). This is a pattern encountered often in the crystal growth in gels [27]. The deposits in the interior were clearly less, in comparison with the respective on the surface of the IOLs in the CCR and their effect on the kinetics measurements was negligible as verified by the constancy of the solution supersaturation.

The formation and subsequent growth of HAP particles on the IOLs under very low flow conditions used in the ECSR yielded results comparable with those obtained in the CCR. The flow of 2.5 mL/day although it simulates the flowrate of the aqueous humor in the eye, is very low but it was enough to maintain the composition of the fluid constant throughout the precipitation process. In situ optical observation and photo capture

provided a means to evaluate the progress of the calcification process (Figure 11). The identification of the deposits could however be verified only by SEM and EDS microanalysis, when the amounts were very low. Measurements of the absorbance of light at 650 nm (Figure 12) offered a means of “translating” transparency with the population density of the HAP deposited on the surface, but saturation, limited the possibility of monitoring the calcification over prolonged time. Moreover, the method required the ex-situ measurement of the samples. As expected, the prolonged residence time of the SAH, supersaturated with respect to HAP, resulted mainly in the formation of subsurface deposits (in addition to deposits on the surface) which appeared as lumps (Figure 13). This situation has been encountered in clinically explanted calcified IOL which became opaque due to the formation of deposits (Figure 14). It seems that the ECSR is a reactor with the potential to simulate biological calcification of IOLs. It needs further exploration, especially in the development of reliable methodology for the assessment of the evolution of the calcification process.

In hydrophilic IOLs, opacification is due to calcification. In the past 25 years, the reports of serial or individual explantations of calcified IOLs come from Hydroview model H60M (Bausch and Lomb, Rochester, NY, USA), SC60B-OUV (MDR Inc, Prescott, AZ, USA), MemoryLens (Ciba Vision Inc, Chicago, IL, USA), and Aqua-Sense (OII Inc, Tierra Verde, FL, USA) and different IOLs model [28,29]. Recently, growing data suggests a causal relationship between endothelial keratoplasty and vitrectomies and hydrophilic IOL calcification. That was more likely caused by an intracameral or intravitreal air or gas injection during the procedure [29,30] Patients with calcified IOLs have progressive deterioration of their visual acuity, and there has not been any evidence of spontaneous recovery, so the only therapeutic approach in such patients is IOL exchange. Unpleasant complications might arise from the explantation of a calcified IOL, sometimes years after the initial cataract surgery [30]. This study may provide a further understanding of IOL calcification in order to prevent its creation or dissolve the precipitation of calcium phosphate crystals for the benefit of patients.

5. Conclusions

Hydrophilic IOLs are calcified, inducing selectively the formation of HAP on their surface and at the interior. The formation of HAP in the IOLs is controlled by surface diffusion as shown by the parabolic dependence of the rates of HAP growth as a function of the relative supersaturation with respect to HAP. The rates of HAP formation were measured at constant driving force in the appropriate reactor (CCR) ensuring accuracy and reproducibility. Calculations of the surface energy of the HAP nuclei from the measured induction times according to CNT, showed dependence on the treatment history of the IOLs. Shorter induction times and lower rates of precipitation of HAP on the IOLs were associated with preparations with higher surface energy. The experimental findings were validated by comparison with clinical findings on surgically explanted IOLs. The use of ECSR, in which the flow of SAH was equal to the corresponding in physiological human eye and the composition of SAH simulated the composition of healthy humans with respect to inorganic components proved to be a reliable model simulating in vivo opacification due to calcification. IOLs calcified both in the CCR and in the ECSR (in both cases at constant supersaturation) showed formation of the deposits in their interior. Most likely supersaturation in the interior of the IOLs is established by diffusion of the mineral component ions. In any case the formation of the solid phase is facilitated by the presence of active sites on the polymeric matrix due to the interaction of the ionized hydroxyl groups with the calcium cations. This was confirmed by measurements of the zeta potential of the PHEMA hydrophilic IOL surface, the value of which was strongly negative, corresponding to deprotonated hydroxyl groups. The calcification of hydrophilic IOLs is possible to be investigated in reactors simulating in vivo situations and reliable screening tests may thus be established.

Supplementary Materials: The following supporting information can be downloaded at: <https://www.mdpi.com/article/10.3390/cryst12101418/s1>, Figure S1: Solubility isotherms calculated for HAP and OCP; 0.15 M NaCl; Total Calcium: Total Phosphate = 1.67. Red circle: Simulated aqueous humor; Blue circles define the limits of calcification experiments in the present work; Figure S2: Left: Photograph of the opacified IOL with HAP deposits. X-ray diffractogram of the calcified hydrophilic IOL; simulated aqueous humor, Total Calcium, Cat = 1.7 mM, Total Phosphate, Pt = 0.6 mM, 0.15 M NaCl, pH 7.40, 37 °C. Upper diffractogram IOL. Lower: Standard from International Center for Diffraction Data (ICDD) PDF-2 Database, Card File No. 9-432 for HAP; Figure S3: Calcification of hydrophilic IOLs below the surface; (a) The surface of the IOLs is characterized by the presence of lumps which contain HAP formed in the interior of the IOL. Bar 2 μ M (b): EDX microanalysis of the lumps on the surface of the IOL showing that they consist of calcium phosphate crystal deposits.

Author Contributions: Conceptualization, P.G.K. and S.P.G.; methodology, P.S.G. and P.D.N.; investigation, P.D.N.; resources, P.G.K. and S.P.G.; data curation, P.S.G. and P.D.N.; writing—original draft preparation, P.S.G. and P.D.N.; writing—review and editing, P.G.K. and S.P.G.; supervision, P.G.K. and S.P.G. All authors have read and agreed to the published version of the manuscript.

Funding: This research received no external funding.

Data Availability Statement: Not applicable.

Acknowledgments: The authors acknowledge the assistance of Christos Kontoyannis, University of Patras, Department of Pharmacy, for micro Raman analyses.

Conflicts of Interest: The authors declare no conflict of interest.

References

1. Lerman, S. The ocular lens. In *Radiant Energy in the Eye*; Lerman, S., Ed.; Macmillan: New York, NY, USA, 1980; pp. 73–93.
2. Apple, D.J.; Sims, J. Harold Ridley and the invention of the intraocular lens. *Surv. Ophthalmol.* **1996**, *40*, 279–292. [[CrossRef](#)]
3. Suh, Y.; Oh, C.; Kim, H.M. Comparison of the long-term clinical results of hydrophilic and hydrophobic acrylic intraocular lenses. *Korean J. Ophthalmol.* **2005**, *19*, 29–33. [[CrossRef](#)]
4. Jensen, M.K.; Crandall, A.S.; Mamalis, N.; Olson, R.J. Crystallization on intraocular lens surfaces associated with the use of Healon GV. *Arch. Ophthalmol.* **1994**, *112*, 1037–1042. [[CrossRef](#)] [[PubMed](#)]
5. Ursell, P.G.; Spalton, D.J.; Pande, M.V.; Hollick, E.J.; Barman, S.; Boyce, J.; Tilling, K. Relationship between intraocular lens biomaterials and posterior capsule opacification. *J. Cataract Refract. Surg.* **1998**, *24*, 352–360. [[CrossRef](#)]
6. Bompastor-Ramos, P.; Póvoa, J.; Lobo, C.; Rodriguez, A.E.; Alió, J.L.; Werner, L.; Murta, J.N. Late postoperative opacification of a hydrophilic-hydrophobic acrylic intraocular lens. *J. Cataract Refract Surg.* **2016**, *42*, 1324–1331. [[CrossRef](#)] [[PubMed](#)]
7. Guan, X.; Tang, R.; Nancollas, G.H. The potential calcification of octacalcium phosphate on intraocular lens surfaces. *J. Biomed. Mater. Res. A* **2004**, *71*, 488–496. [[CrossRef](#)] [[PubMed](#)]
8. Rezaei-Kanavi, M.; Javadi, M.A.; Mirbabaei-Ghafghazi, F. Intraocular lens calcification; A clinicopathologic report. *J. Ophthalmic Vis. Res.* **2009**, *4*, 122–124.
9. Izak, A.; Werner, L.; Pandey, S.; Apple, D.J. Calcification of modern foldable hydrogel intraocular lens designs. *Eye* **2003**, *17*, 393–406. [[CrossRef](#)]
10. Koutsoukos, P.G.; Amjad, Z.; Tomson, M.B.; Nancollas, G.H. Crystallization of calcium phosphates. A constant composition study. *J. Amer. Chem. Soc.* **1980**, *102*, 1553–1557. [[CrossRef](#)]
11. Dalas, E.; Kallitsis, J.; Koutsoukos, P.G. The growth of sparingly soluble salts on polymeric substrates. *Colloids Surf.* **1991**, *53*, 197–208. [[CrossRef](#)]
12. Gurabardhi, M.; Häberle, H.; Aurich, H.; Werner, L.; Pham, D.T. Serial intraocular lens opacifications of different designs from the same manufacturer: Clinical and light microscopic results of 71 explant cases. *J. Cataract Refract. Surg.* **2018**, *44*, 1326–1332. [[CrossRef](#)]
13. Nagul, E.A. The molybdenum blue reaction for the determination of orthophosphate revisited: Opening the black box. *Anal. Chim. Acta* **2015**, *890*, 60–82. [[CrossRef](#)] [[PubMed](#)]
14. Bates, R.G. Revised Standard Values for pH Measurements from 0 to 95 °C. *J. Res. N Bur. Stan. A-Phys. Chem.* **1962**, *66A*, 179–184. [[CrossRef](#)]
15. Drimtzias, E.G.; Rokidi, S.G.; Gartaganis, S.P.; Koutsoukos, P.G. Experimental investigation on mechanism of hydrophilic acrylic intraocular lens calcification. *Am. J. Ophthalmol.* **2011**, *152*, 824–833.e1. [[CrossRef](#)]
16. Kinsey, V.E. Comparative chemistry of aqueous humor in posterior and anterior chambers of rabbit eye. Its physiologic significance. *A.M.A. Arch. Ophthalmol.* **1953**, *50*, 401–417.
17. Christoffersen, J.; Christoffersen, M.R.; Kibalczyk, W.; Andersen, F.A. A contribution to the understanding of the formation of calcium phosphates. *J. Cryst. Growth* **1989**, *94*, 767–777. [[CrossRef](#)]

18. Ding, H.; Pan, H.; Xu, X.; Tang, R. Towards a Detailed Understanding of Magnesium ions on Hydroxy-yapatite Crystallization Inhibition. *Cryst. Growth Des.* **2014**, *14*, 763–769. [[CrossRef](#)]
19. Skartsila, K.; Spanos, N. Physicochemical characterization of variously packed porous plugs of hydroxyapatite: Streaming potential coupled with conductivity measurements. *Langmuir* **2006**, *22*, 1903–1910. [[CrossRef](#)]
20. Spanos, N.; Misirlis, D.Y.; Kanellopoulou, D.G.; Koutsoukos, P.G. Seeded growth of hydroxyapatite in simulated body fluid. *J Mater Sci.* **2003**, *41*, 1805–1812. [[CrossRef](#)]
21. Tao, J.H.; Fijneman, A.; Wan, J.Q.; Prajapati, S.; Mukherjee, K.; Fernandez-Martinez, A.; Moradian-Oldak, J.; De Yoreo, J.J. Control of calcium phosphate nucleation and transformation through interactions of enamel and amelogenin exhibits the “goldilocks effect”. *Cryst. Growth Des.* **2018**, *18*, 7391–7400. [[CrossRef](#)]
22. Fowler, B.O.; Markovic, M.; Brown, W.E. Octacalcium phosphate. 3. Infrared and Raman vibrational spectra. *Chem. Mater.* **1993**, *5*, 1417–1423. [[CrossRef](#)]
23. De Yoreo, J.J.; Vekilov, P. Principles of crystal nucleation and growth. *Rev. Mineral. Geochem.* **2003**, *54*, 57–93. [[CrossRef](#)]
24. Nielsen, A.E. Nucleation in aqueous solutions. In *Crystal Growth*; Peiser, S., Ed.; Pergamon: Oxford, UK, 1967; pp. 419–426.
25. Ibarra-Montaña, E.L.; Rodríguez-Laguna, N.; Sánchez-Hernández, A.; Rojas-Hernández, A. Determination of pKa Values for Acrylic, Methacrylic and Itaconic Acids by ^1H and ^{13}C NMR in Deuterated Water. *J. Appl. Sol. Chem. Model.* **2015**, *4*, 7–18. [[CrossRef](#)]
26. Gartaganis, S.P.; Kanellopoulou, D.G.; Mela, E.K.; Panteli, V.S.; Koutsoukos, P.G. Opacification of hydrophilic acrylic intraocular lens attributable to calcification: Investigation on mechanism. *Am. J. Ophthalmol.* **2008**, *146*, 395–403. [[CrossRef](#)]
27. Gartaganis, S.P.; Prahs, P.; Lazari, E.D.; Gartaganis, P.S.; Helbig, H.; Koutsoukos, P.G. Calcification of Hydrophilic Acrylic Intraocular Lenses With a Hydrophobic Surface: Laboratory Analysis of 6 Cases. *Am. J. Ophthalmol.* **2016**, *168*, 68–77. [[CrossRef](#)] [[PubMed](#)]
28. Schrittenlocher, S.; Schaub, F.; Hos, D.; Siebelmann, S.; Cursiefen, C.; Bachmann, B. Evolution of Consecutive Descemet Membrane Endothelial Keratoplasty Outcomes Throughout a 5-Year Period Performed by Two Experienced Surgeons. *Am. J. Ophthalmol.* **2018**, *190*, 171–178. [[CrossRef](#)] [[PubMed](#)]
29. Belin, P.J.; Kim, J.H.; Sheikh, A.; Winokur, J.; Rhee, D.; Deramo, V. Incidence and Risk of Scleral-Fixated Akreos (AO60) Lens Opacification: A Case Series. *J. Vitre. Retinal. Dis.* **2021**, *5*, 157–162. [[CrossRef](#)]
30. Fernández-Buenaga, R.; Alió, J.L. Intraocular Lens Explantation After Cataract Surgery: Indications, Results, and Explantation Techniques. *Asia Pac. J. Ophthalmol.* **2017**, *6*, 372–380. [[CrossRef](#)] [[PubMed](#)]